RSC Advances

ROYAL SOCIETY OF CHEMISTRY

www.rsc.org/advances

Enhanced near-infrared emission by co-doping Ce^{3+} in $Ba_2Y(BO_3)_2Cl$: Tb^{3+}, Yb^{3+} phosphor

Jin Zhao, Chongfeng Guo*, and Ting Li

National Key Laboratory of Photoelectric Technology and Functional Materials (Culture Base) in Shaanxi Province, National Photoelectric Technology and Functional Materials & Application of Science and Technology International Cooperation Base, Institute of Photonics & Photon-Technology, Northwest University, Xi'an 710069, China

---

* Author to whom correspondence should be addressed

Institute of Photonics & Photon-Technology;

Northwest University,

Xi'an 710069, China.

Tel. & Fax.: 86-29-88302661

E-mail: guocf@nwu.edu.cn (Prof. Guo)

Abstract: Ce^{3+}-Tb^{3+}-Yb^{3+} tri-doped $Ba_2Y(BO_3)_2Cl$ phosphors with intense near-infrared (NIR) emission and broad band absorption in the near ultraviolet region were synthesized by a convenient solid-state reaction in a reducing atmosphere, and the structure and the phase purity of all samples were characterized using X-ray diffraction (XRD). The visible and NIR emission spectra companied with corresponding decay curves have also been measured to investigate the energy transfer (ET) processes and analysis ET mechanisms and efficiencies in Ce^{3+}-Tb^{3+}-Yb^{3+} tri-doped system. In addition, steady and dynamic luminescent properties of Tb^{3+}/Ce^{3+}-Yb^{3+} co-doped $Ba_2Y(BO_3)_2Cl$ phosphors were also measured as contrasts. As an excellent sensitizer, Ce^{3+} ion could enormously enlarge the absorption cross-section and greatly enhance the NIR emission intensity of Yb^{3+} ion. It is believed that Ce^{3+}-Tb^{3+}-Yb^{3+} tri-doped $Ba_2Y(BO_3)_2Cl$ phosphor is a promising down-conversion (DC) solar spectral convertor to enhance the efficiency of the silicon solar cells.

Keywords: Solar cells; Phosphor; Down-conversion; Energy transfer.

1. Introduction

Due to the global energy crisis, much attention has been paid to green and renewable energy. Solar cells are recognized as the most promising devices those convert the solar energy to electricity, while silicon solar cells occupy the dominant position in the solar market.[1-3] The major energy loss in crystalline Si (c-Si) solar cell is spectral mismatch between the incident solar spectrum and silicon spectral response, which is the main reason for the lower photoelectric conversion efficiency.[4] The photons with lower energy than the band gap (Eg ≈1.12 eV, λ≈1100 nm) of silicon are not absorbed, while the photons with much higher energy than the band gap loss their excess energy through thermalization of hot charge carriers.[5] A promising method to reduce the thermalization effect is to turn one ultraviolet-visible (UV-Vis) high energy photon into one or more available near infrared (NIR) low energy photons via down-conversion (DC) luminescent materials, including down shift (DS, shift short-wavelength light to long-wavelength light) and quantum cutting (QC, split one incident high energy photon into two near infrared photons) two processes. Since efforts are being made to enhance the efficiency of silicon solar cells, the highest efficiency is not limited to 30% (the Schockley–Queisser limit) via spectral modification with DC phosphors.[6-7]

Recently, RE^{3+}-Yb^{3+} (RE=Tb^{3+}, Pr^{3+}, Tm^{3+}, Ho^{3+} or Er^{3+}) ion pairs co-doped QC materials have been extensively investigated, in which Yb^{3+} ion is a suitable emitter and acceptor with its around 1000 nm NIR emission and matches well with the band gap of c-Si due to its simple energy levels of $^2F_{5/2}$ and $^2F_{7/2}$ (separated by ~10000 cm^{-1}).[8] According to the quantum cutting concept, one blue photon absorbed by RE^{3+} due to the absorption of Tb^{3+}: $^7F_6 \rightarrow {}^5D_4$ around 486 nm, Pr^{3+}: $^3H_4 \rightarrow {}^3P_2$ around 445 nm, Ho^{3+}: $^5F_3 \rightarrow {}^5I_8$ around 447 nm and so on could be divided into two NIR photons of Yb^{3+} ion by the $^2F_{5/2} \rightarrow {}^2F_{7/2}$ transition, which may lower the adverse thermalization effect caused by excess energy.[9] However, these RE^{3+} ions suffer from narrow absorption cross sections (in the order of 10^{-21} cm^2) and low absorption intensity due to the forbidden 4f-4f transitions. Thus, the NIR emission from Yb^{3+} is so weak that application of RE^{3+}-Yb^{3+} (RE=Tb^{3+}, Pr^{3+}, Tm^{3+}, Ho^{3+} or Er^{3+}) co-doped QC materials in silicon solar cells is limited.[10-13] Unlike other RE^{3+} ions, Ce^{3+} ions with the allowed 4f-5d transitions generally have broad and strong absorption (in an order of 10^{-18} cm^2) in the UV-Vis region.[14] Ce^{3+} ion could be used as an efficient sensitizer and transfer its energy absorbed from the UV-Vis region to Tb^{3+} or

Yb^{3+} effectively.[15] In addition, cooperative energy transfer (CET) mechanisms of $RE^{3+} \rightarrow 2Yb^{3+}$ (e.g. RE= Ce^{3+}, Tb^{3+}, Pr^{3+}, Tm^{3+}) were theoretically realizable and had been investigated in detail, which is a possible way of energy transfer (ET) in RE^{3+}-Yb^{3+} pair.[16-17] According to our previous result, the phosphor $Ba_2Y(BO_3)_2Cl$: Ce^{3+}, Tb^{3+} exhibited both a blue emission from Ce^{3+} and a green emission from Tb^{3+} under near ultraviolet light excitation with range of 320-390 nm, energy transfer from Ce^{3+} to Tb^{3+} was efficient.[18] Therefore, it is possible to occur for the energy transfer from Ce^{3+} to Tb^{3+}-Yb^{3+} ion pairs.

In this paper, we investigated the Ce^{3+}-Tb^{3+}-Yb^{3+} tri-doped $Ba_2Y(BO_3)_2Cl$ phosphor. The visible and NIR emission spectra and corresponding decay curves were measured to prove the occurrence of ET in present system, and the ET mechanisms were systematically studied and discussed. The results demonstrate that Ce^{3+} ion could efficiently sensitize the Tb^{3+}-Yb^{3+} pair and enhance the NIR emission of Yb^{3+} ion greatly.

2. Experimental

All the $Ba_2Y(BO_3)_2Cl$: Tb^{3+}/Ce^{3+}, Yb^{3+} and $Ba_2Y(BO_3)_2Cl$: Ce^{3+}, Tb^{3+}, Yb^{3+} powder samples were prepared by a conventional solid-state reaction in a reducing atmosphere. Analytical grade $BaCO_3$, $BaCl_2 \cdot 2H_2O$, H_3BO_3 (excess 5 mol% to compensate for the evaporation), and high purity (99.99%) rare earth oxides Y_2O_3, Yb_2O_3, Tb_4O_7, CeO_2 were used as raw materials. The composition for each sample was weighted in proper stoichiometric ratio and mixed thoroughly in an agate mortar. The mixture samples were preheated at 500 ℃ for 2 h in air. After being cooled to room temperature, the sample was thoroughly reground and heated for 4 h in the CO atmosphere at 900 ℃ to insure the complete reduction of Ce^{3+} and Tb^{3+}. It was then cooled to room temperature and crushed into fine powder.

The X-ray diffraction (XRD) patterns were performed on Rigaku-Dmax 3C powder diffractometer (Rigaku Corp, Tokyo, Japan) with Cu-Kα radiation (λ = 1.54065 Å) to identify the structure and phase purity. The photoluminescence emission (PL) and excitation (PLE) spectra and decay curves were recorded by an Ediburgh FLS920 spectrofluorometer and a 450W Xe lamp was used as excitation source. Decay curve measurements of Ce^{3+} ion were obtained using a 375 nm nanosecond flash-lamp (nF900) as the excitation source. Photoluminescent spectra of all samples were tested three times to reduce the error and all of the measurements were performed at room

temperature.

3. Results and discussions

3.1 Phase and structure

Figure 1 representatively shows the X-ray diffraction (XRD) patterns of Tb^{3+} solely doped, Tb^{3+}-Yb^{3+} co-doped and Ce^{3+}-Tb^{3+}-Yb^{3+} tri-doped $Ba_2Y(BO_3)_2Cl$ samples. The diffraction peaks of all samples agree well with those of the standard profile (JCPDS No. 79-0967) $Ba_2Yb(BO_3)_2Cl$ and no any diffraction peaks from impurity. It is noted that all samples show similar XRD patterns in our experiments, which indicate that the obtained samples are single and pure phase, and RE^{3+} (Ce^{3+}/Tb^{3+}/Yb^{3+}) ions are completely enter the lattices even though at high concentrations. Here, most of the rare earth ion dopants would prefer to occupy Y^{3+} site in the $Ba_2Y(BO_3)_2Cl$ compound according to the close effective ionic radius and valence of the cations. The compound $Ba_2Y(BO_3)_2Cl$ shares the same structure with $Ba_2Yb(BO_3)_2Cl$, which crystallizes in a monoclinic structure with the space group $P2_1/m$, having the lattice parameters of a = 6.397 Å, b = 5.279 Å, c =11.222 Å.[19]

3.2 Analysis of photoluminescence spectra and energy transfer processes

3.2.1 Luminescence and ET in Tb^{3+}-Yb^{3+} or Ce^{3+}-Yb^{3+} codoped $Ba_2Y(BO_3)_2Cl$

Photoluminescence excitation (PLE) and emission (PL) spectra of the $Ba_2Y(BO_3)_2Cl$: $0.03Tb^{3+}$, $0.20Yb^{3+}$ and $Ba_2Y(BO_3)_2Cl$: $0.03Ce^{3+}$, $0.20Yb^{3+}$ samples are presented in Fig. 2a and b, respectively. Monitoring the characteristic green emission of Tb^{3+} at 542 nm, PLE spectrum shown in Fig. 2a consists of a weak band around 280 nm and several weak peaks in the 300-500 nm due to the lowest spin-forbidden 4f→5d transitions and the forbidden 4f→4f transitions of Tb^{3+} ion.[20] The amplifying excitation peak centered at 486 nm is assigned to Tb^{3+}: $^7F_6 \rightarrow {}^5D_4$ transition, which usually used as excitation peak in Tb^{3+}-Yb^{3+} co-doped quantum cutting systems.[21] The excitation spectrum profile monitoring at 972 nm from the $^2F_{5/2} \rightarrow {}^2F_{7/2}$ transition of Yb^{3+} is similar to that of monitoring at 542 nm, which indicates the occurrence of ET from Tb^{3+} to Yb^{3+}, and the trivial difference might be from different detectors of Vis and NIR spectrum measurement. Herein, both the emission and inset excitation intensities of Tb^{3+} ion are magnified 40 times for the sake of clarify. Under blue excitation at 486 nm, emissions peaking at 542, 583, 620 nm are observed, which can be assigned to the forbidden $^5D_4 \rightarrow {}^7F_J$ (J=5, 4, 3) transitions of

Tb^{3+}.[22] Meanwhile, the characteristic NIR emission band located at 900-1150 nm is also observed, due to the $^2F_{5/2}\rightarrow{}^2F_{7/2}$ transition of Yb^{3+}. The NIR emission spectra separately excited by 355 nm and 486 nm are shown in the insert of Fig. 2a, and the former integrated intensity is 6 times of the latter. With the increasing of Yb^{3+}concentration, it is clearly found that the emission intensities of Tb^{3+} rapidly decrease while the Yb^{3+} NIR emission intensities grow simultaneously, as shown in Fig. 2c, which further confirms the occurrence of ET from Tb^{3+} to Yb^{3+}.

Figure 2b exhibits the PLE and PL spectra of $Ba_2Y(BO_3)_2Cl$: $0.03Ce^{3+}$, $0.20Yb^{3+}$ phosphor. Upon 355 nm excitation, the phosphor generates the blue emission from Ce^{3+} and NIR emission from Yb^{3+}. For the PLE spectra monitoring both the 5d→4f transition of Ce^{3+} at 417 nm and the $^2F_{5/2}\rightarrow{}^2F_{7/2}$ transition of Yb^{3+} at 972 nm, they are similar except intensity concluding an intense excitation band of Ce^{3+}: 4f→5d centered at 355 nm, which indicates the energy transfer from Ce^{3+} to Yb^{3+}.[23] It is observed that the emission of Ce^{3+} decreases and the emission of Yb^{3+} increases with increasing the contents of Yb^{3+}, whereas the emission intensity of Yb^{3+} reaches the maximum at x=0.2 due to concentration quenching effect (as shown in Fig. 2d). Regular changes emission intensities from Ce^{3+} or Yb^{3+} also provide the powerful evidence for the ET process from Ce^{3+} to Yb^{3+}.

In order to further prove the occurrence of the energy transfer from Tb^{3+}/Ce^{3+} to Yb^{3+} and well understand the ET process, the decay curves of the Tb^{3+}: $^5D_4\rightarrow{}^7F_5$ emission at 542 nm in $Ba_2Y(BO_3)_2Cl$: $0.03Tb^{3+}$, xYb^{3+} and the Ce^{3+}: 5d→4f emission at 417 nm in $Ba_2Y(BO_3)_2Cl$: $0.03Ce^{3+}$, xYb^{3+} were recorded in Fig. 3a and b. The Tb^{3+} 542 nm emission without Yb^{3+} shows a nearly single exponential decay, whereas the Ce^{3+} 417 nm emission without Yb^{3+} deviates from single exponential decay because of the energy transfer between possible distribution of Ce^{3+} in different cation sites (two Ba^{2+} cites and one Y^{3+} site).[14] For the sample without any Yb^{3+}, the decay time of 3.46 ms and 20.31 ns are obtained for Tb^{3+} and Ce^{3+} by fitting. As the introduction of Yb^{3+} and increasing its concentration, their decay curves became nonexponential and the lifetime of the sensitizer Tb^{3+} or Ce^{3+} decreases. The average lifetime (τ) of sensitizer Tb^{3+}/Ce^{3+} in Tb^{3+}/Ce^{3+}-Yb^{3+} co-doped $Ba_2Y(BO_3)_2Cl$ samples is given by:[24]

$$\tau = \int_0^\infty tI_{(t)}dt \Big/ \int_0^\infty I_{(t)}dt \quad (1)$$

where $I_{(t)}$ is the luminescence intensity at time t. The decay life time of Tb^{3+}/Ce^{3+} drops gradually with Yb^{3+} co-doping, and their lifetimes are about 3.40, 3.33, 3.32, 3.08, 2.73 ms and 10.44, 4.90, 2.83, 2.38, 1.38 ns for Tb^{3+} and Ce^{3+} in $0.03Tb^{3+}$-xYb^{3+} or $0.03Ce^{3+}$-xYb^{3+} co-doped $Ba_2Y(BO_3)_2Cl$, respectively.

Figure 3c and d present the emission average lifetime and energy transfer efficiency of Tb^{3+}/Ce^{3+}-Yb^{3+} co-doped $Ba_2Y(BO_3)_2Cl$ samples as function of Yb^{3+} concentrations. According to the decay times, the energy transfer efficiency (ETE, η_{ETE}) can be calculated by using the following equations:[25]

$$\eta_{ETE} = 1 - \tau_{xYb} / \tau_{0Yb} \quad (2)$$

where τ_{xYb} and τ_{0Yb} denote lifetime of the sensitizer with and without Yb^{3+} content. Accordingly, the ET efficiency (η_{ETE}) are 2.0, 3.8, 4.0, 11.0, 21.1% for $Ba_2Y(BO_3)_2Cl$: $0.03Tb^{3+}$, xYb^{3+} and 48.6, 75.9, 86.1, 88.3 and 93.2% for $Ba_2Y(BO_3)_2Cl$: $0.03Ce^{3+}$, xYb^{3+} with increasing the content of Yb^{3+} from 0.01 to 0.3, respectively. The η_{ETE} value rises monotonously with increasing Yb^{3+} doping content, but the ET efficiency is much lower in $Ba_2Y(BO_3)_2Cl$: $0.03Tb^{3+}$, xYb^{3+} than that of in $Ba_2Y(BO_3)_2Cl$: $0.03Ce^{3+}$, xYb^{3+}, which may be due to the lower and inefficient forbidden 4f→4f absorption cross-sections of Tb^{3+} in UV-visible region than that of the allowed 4f→5d of Ce^{3+}. It could be expected that the NIR emission intensity is stronger in Ce^{3+}-Yb^{3+} co-doped $Ba_2Y(BO_3)_2Cl$ than that of in Tb^{3+}-Yb^{3+} co-doped $Ba_2Y(BO_3)_2Cl$, which will be discussed in the following paragraph. In addition, it is found that the energy transfer efficiency of Ce^{3+}→Yb^{3+} is much higher than that of Ce^{3+}→Tb^{3+} in comparison with that of our previous results,[18] which indicates that the energy absorbed by Ce^{3+} is more easily transfer to Yb^{3+}.

3.2.2 Luminescence in Ce^{3+}-Tb^{3+}-Yb^{3+} tri-doped $Ba_2Y(BO_3)_2Cl$ phosphor

According to above mentioned and previous results, the energy transfer Ce^{3+}→Tb^{3+} and Tb^{3+}→Yb^{3+} have occurred in the $Ba_2Y(BO_3)_2Cl$ host, it is possible to take place for the energy transfer from Ce^{3+} to Tb^{3+}→Yb^{3+} ion pairs. Figure 4 displays the PLE and PL spectra of Ce^{3+}-Tb^{3+}-xYb^{3+} tri-doped $Ba_2Y(BO_3)_2Cl$ phosphor. As the representative PLE spectra (shown in Fig. 4a), they include a broad excitation band at 320-390 nm with a maximum at 355 nm corresponding to the Ce^{3+}: 4f→5d transition. It is found that the profiles of PLE spectra obtained by monitoring at 542 nm (Tb^{3+}: $^5D_4$→$^7F_5$ emission), 417 nm (Ce^{3+}: 5d→4f emission) and 972 nm

(Yb^{3+}: $^2F_{5/2}\rightarrow{}^2F_{7/2}$ emission) are similar to that of Ce^{3+} solely doped $Ba_2Y(BO_3)_2Cl$ except relative intensity, which illuminates that the possible appearance of energy transfer from Ce^{3+} to Tb^{3+}/Yb^{3+}/Tb^{3+}-Yb^{3+}. Under the excitation of 355 nm light, the PL spectra of $Ba_2Y(BO_3)_2Cl$: $0.03Ce^{3+}$, $0.03Tb^{3+}$, xYb^{3+} in visible and near infrared region as function of Yb^{3+} contents are shown in Fig. 4b. The PL spectra are composed of a typical broad unsymmetrical doublet emission bands from the parity-allowed transitions from the 5d excited state to the $^2F_{7/2}$ and $^2F_{5/2}$ ground states of Ce^{3+} [26] and a series of sharp lines emission in 480-680 nm region from the $^5D_4\rightarrow{}^7F_J$ (J=6, 5, 4 and 3) tansitions of Tb^{3+} in visible region, as well as the NIR emission band centered at 972 nm accompanied by several weak shoulders in 900-1150 nm region due to transitions among the different stark levels of ^2F_J (J=5/2, 7/2) of Yb^{3+}. Seen from the PL spectra, it is observed that the intensity of Tb^{3+} emission (integrated from 480 to 680 nm) and Ce^{3+} emission (integrated from 370 to 480 nm) decreases monotonously with the increase of Yb^{3+} concentration from 0 to 0.3, while the NIR emission intensity of Yb^{3+} (integrated from 900 to 1150 nm) firstly increases with Yb^{3+} content growth and then begins to decrease after reaching the maximum at x=0.20 due to concentration quenching effect. In order to clearly illuminate variation, inset of Fig. 4b displays the variable curves of normalized PL intensity from Ce^{3+}, Tb^{3+} and Yb^{3+} on the Yb^{3+} concentration x, respectively.

The energy transfer process is complicated in Ce^{3+}-Tb^{3+}-Yb^{3+} tri-doped $Ba_2Y(BO_3)_2Cl$ sample. To further understand the energy transfer in this system, the decay curves of the sensitizer Ce^{3+} and Tb^{3+} in sample $Ba_2Y(BO_3)_2Cl$: $0.03Ce^{3+}$, $0.03Tb^{3+}$, xYb^{3+} (x=0-0.3) are plotted on the concentration of Yb^{3+}, those are shown in Fig. 5. With increasing Yb^{3+} concentration, the decay of Ce^{3+} and Tb^{3+} ($^5D_4$) in tri-doped $Ba_2Y(BO_3)_2Cl$: $0.03Ce^{3+}$, $0.03Tb^{3+}$, xYb^{3+} sample speed up (as shown in Fig. 5a and b), similar to those in co-doped $Ba_2Y(BO_3)_2Cl$: $0.03Ce^{3+}$, xYb^{3+} and $Ba_2Y(BO_3)_2Cl$: $0.03Tb^{3+}$, xYb^{3+}. The effective decay times are calculated to be about 12.82, 9.63, 2.89, 2.60, 1.77, 1.28 ns for Ce^{3+} and 3.56, 3.26, 3.18, 3.06, 2.77, 2.48 ms for Tb^{3+}, therefore the η_{ETE} values are 36.8, 52.6, 85.8, 87.2, 91.2, 93.7% ($\eta_{ETE\text{-}Ce}$) and 0, 8.6, 10.7, 14.0, 22.2, 30.3% ($\eta_{ETE\text{-}Tb}$) according to the decline of Ce^{3+} and Tb^{3+} lifetime, respectively. The corresponding lifetimes and energy transfer efficiency variable curves as function of Yb^{3+} contents are also shown clearly in Fig. 5c and d, in there the $\eta_{ETE\text{-}Ce}$ values calculated on the basis of the decrease of Ce^{3+} lifetime are not started from 0 whereas the $\eta_{ETE\text{-}Tb}$ values are started from 0. Because $\eta_{ETE\text{-}Ce}$

value is the sum of ET efficiency of Ce^{3+}→Tb^{3+} and Ce^{3+}→Yb^{3+}, but $\eta_{ETE\text{-}Tb}$ is the only ET efficiency value of Tb^{3+}→Yb^{3+}. Comparison with that of the co-doped system, it is found that the ET efficiency was higher in tri-doped sample than those of corresponding co-doped samples. Thus we deduced that the NIR emission intensity in $Ba_2Y(BO_3)_2Cl$: $0.03Ce^{3+}$, $0.03Tb^{3+}$, xYb^{3+} should be stronger than that of corresponding $Ba_2Y(BO_3)_2Cl$: $0.03Ce^{3+}$, xYb^{3+} or $Ba_2Y(BO_3)_2Cl$: $0.03Tb^{3+}$, xYb^{3+}, which is strongly related to the energy transfer processes.

3.2.3 Energy transfer processes in Ce^{3+}-Tb^{3+}-Yb^{3+} tri-doped $Ba_2Y(BO_3)_2Cl$

Based on above mentioned results, the possible ET processes were analyzed in detail by schematic energy level diagram with feasible transitions, which are shown in Fig. 6. In the present Ce^{3+}-Tb^{3+}-Yb^{3+} tri-doped system, the possible energy transfer processes include Ce^{3+}→Yb^{3+}, Ce^{3+}→Tb^{3+}, Tb^{3+}→Yb^{3+} and Ce^{3+}→Tb^{3+}→Yb^{3+} four procedures. For the first energy transfer process ① Ce^{3+}→Yb^{3+}, it is usually considered that the cooperative down-conversion (or quantum cutting, QC) probably dominates the process because the energy of Ce^{3+}: 5d→4f transition is beyond twice as high as the energy difference between the $^2F_{7/2}$ and $^2F_{5/2}$ levels of Yb^{3+}.[27] Up to now, no direct experimental proof could support the existence or inexistence of QC, whereas many measured Yb^{3+} quantum yield (QY) in the samples with so called "QC" are far below 100%.[28-29] The authors considered the ET Ce^{3+} to Yb^{3+} may include both Ce^{3+}→$2Yb^{3+}$ (1a) and Ce^{3+}→Yb^{3+} (1b) two processes: the former is a CET process and possible existence in theory, and the latter is possibly through a slow non-radiative relaxation from an intermediate Ce^{4+}–Yb^{2+} charge transfer state companied with energy loss instead of directly via Ce^{3+}: 5d→$2Yb^{3+}$: $^2F_{5/2}$.[29-31] The energy transfer processes ② Ce^{3+}→Tb^{3+} have been investigated in many hosts,[32, 33] in which part of excited energy of Ce^{3+} could transfer to Tb^{3+} due to the Ce^{3+} excited 5d state energy level is close to that of the $^5D_3$ and $^5D_4$ of Tb^{3+}, resonant energy transfer could take place and promote the electrons of Tb^{3+} from $^7F_6$ ground state to $^5D_3$ and other excited levels. Then non-radiative relaxation occurs from the high energy levels $^5D_3$ to the $^5D_4$ levels, resulting in several sharp line emissions from $^5D_4$→^7F_J (J=6, 5, 4 and 3) tansitions of Tb^{3+} and peaking 486, 542, 583 and 620 nm, respectively (2).[34] For the energy transfer ③ Tb^{3+}→Yb^{3+}, the energy of Tb^{3+} ($^5D_4$) level is approximately two times as high as the energy difference between the $^2F_{7/2}$ and $^2F_{5/2}$ levels of Yb^{3+}, which probably makes CET or QC process Tb^{3+} ($^5D_4$) →$2Yb^{3+}$ ($^2F_{5/2}$) occur, the energy of the excited Tb^{3+} ion is transferred to two different Yb^{3+} ions (3a). A Tb^{3+}–Yb^{3+} cross-relaxation

mechanism is also possible to excite one Yb^{3+} with a subsequent energy loss through multi-phonon decay process in Tb^{3+} ion (3b).[35] On the basis of above mentioned three ET processes, the fourth energy transfer ④ $Ce^{3+}\rightarrow Tb^{3+}\rightarrow Yb^{3+}$ is easy to understand, upon excitation by 355 nm n-UV light, the Ce^{3+} ion in the ground state $^2F_{5/2}$ is excited to higher excited state 5d level, part of the excited state electrons relax to the ground state $^2F_{5/2}$ and $^2F_{7/2}$ of Ce^{3+} in the form of broad band blue emissions, part of the excited state elctrons energy transfer to Tb^{3+}, then the part of the accepted energy of Tb^{3+} transfer to Yb^{3+} exhibiting the NIR emission of Yb^{3+}: $^2F_{5/2}\rightarrow{}^2F_{7/2}$. Here, Tb^{3+} ions play the role of bridge to form a new energy transfer pathway. Yb^{3+} NIR emission could involve four energy transfer processes in Ce^{3+}-Tb^{3+}-Yb^{3+} tri-doped $Ba_2Y(BO_3)_2Cl$.

3.2.4 Comparison of NIR emission in the co-doped and tri-doped samples

The aim of the present paper is to enhance the NIR emission from Yb^{3+} transitions through the Ce^{3+}-Tb^{3+}-Yb^{3+} ion pairs tri-doped $Ba_2Y(BO_3)_2Cl$ sample. In order to compare NIR emission intensity in co-doped system with that of in tri-doped, Fig. 7 shows the PL spectra in NIR region of $0.03Tb^{3+}$, $0.20Yb^{3+}$ and $0.03Ce^{3+}$, $0.20Yb^{3+}$ co-doped $Ba_2Y(BO_3)_2Cl$, as well as $Ba_2Y(BO_3)_2Cl$: $0.03Ce^{3+}$, $0.03Tb^{3+}$, $0.20Yb^{3+}$ sample with optimal composition. It is observed that the NIR emission intensity of samples doped with Tb^{3+} under the excitation of 486 nm (Tb^{3+}: $^7F_6\rightarrow{}^5D_4$) is lower than that of samples excited with 355 nm, which due to the weak absorption and narrow absorption cross-section of Tb^{3+} at 486 nm. Under the excitation of 355 nm, NIR emission intensity increases with the order $I_{Tb\text{-}Yb}< I_{Ce\text{-}Yb}< I_{Ce\text{-}Tb\text{-}Yb}$, which is consistent with the results of the energy transfer efficiency. Meanwhile, the NIR emission integrated intensity of Yb^{3+} ion in tri-doped Ce^{3+}-Tb^{3+}-Yb^{3+} system is 1.4 times of the co-doped Ce^{3+}-Yb^{3+} sample and 23 times as much as that of the co-doped Tb^{3+}-Yb^{3+} sample, which confirms the highly efficient excitation and subsequent $Ce^{3+}\rightarrow Yb^{3+}$, $Tb^{3+}\rightarrow Yb^{3+}$ and $Ce^{3+}\rightarrow Tb^{3+}\rightarrow Yb^{3+}$ possible ET processes in the tri-doped Ce^{3+}-Tb^{3+}-Yb^{3+} material. Results reveal that the introduction of Ce^{3+} as a sensitizer with large absorption cross-section could efficiently turn the adverse high energy photons in near ultraviolet region into favorable low energy NIR photons effectively absorbed by silicon solar cells. The Ce^{3+}-Tb^{3+}-Yb^{3+} tri-doped sample could be a potential DC solar spectral convertor by reducing the energy loss to improve the photoelectric conversion efficiency of silicon solar cells.

4. Conclusions

In summary, steady and dynamic photoluminescent properties and the energy transfer mechanism in the Ce^{3+}-Tb^{3+}-xYb^{3+} tri-doped $Ba_2Y(BO_3)_2Cl$ phosphor were systematically investigated, in there the possible four ET processes $Ce^{3+}\rightarrow Tb^{3+}$, $Ce^{3+}\rightarrow Yb^{3+}$, $Tb^{3+}\rightarrow Yb^{3+}$ and $Ce^{3+}\rightarrow Tb^{3+}\rightarrow Yb^{3+}$ were proposed. As a comparison, the Ce^{3+}/Tb^{3+}-xYb^{3+} co-doped $Ba_2Y(BO_3)_2Cl$ were also studied. It is found that the energy transfer efficiency of $Ce^{3+}\rightarrow xYb^{3+}$ and $Tb^{3+}\rightarrow xYb^{3+}$ in tri-doped system is larger than that of in double doped system. The NIR emission intensity of Yb^{3+} in tri-doped sample under the excitation of 355 nm is 1.4 times of Ce^{3+}-Yb^{3+} co-doped sample and is 23 times of Tb^{3+}-Yb^{3+} co-doped phosphors with optimal composition. Moreover, Ce^{3+} ion enormously enlarges the absorption cross-section in the near ultraviolet region (320-390 nm) due to the allowed 4f→5d transition and greatly enhances the NIR emission of Yb^{3+} ion where the c-Si solar cell exhibits the greatest spectral response. Results indicate that $Ba_2Y(BO_3)_2Cl$: Ce^{3+}, Tb^{3+}, Yb^{3+} phosphor is a promising spectral convertor for enhancing the photoelectric conversion efficiency of silicon solar cells.

Acknowledgments

This work was supported by the high-level talent project of Northwest University, National Natural Science Foundation of China (No. 11274251), Ph.D. Programs Foundation of Ministry of Education of China (20136101110017), Technology Foundation for Selected Overseas Chinese Scholar, Ministry of Personnel of China (excellent), Natural Science Foundation of Shaanxi Province (No.2014JM1004) and Foundation of Key Laboratory of Photoelectric Technology in Shaanxi Province (12JS094).

References

1 O. Morton. Nature, 2006, **443**, 19-22.

2 A. Kraft, C. Wolf, J. Bartsch, M. Glatthaar and S. Glunz, Sol. Energ. Mat. Sol. C., 2015, **136**, 25-31.

3 B. M. van der Ende, L. Aarts and A. Meijerink, Phys. Chem. Chem. Phys., 2009, **11**, 11081-11095.

4 B.S. Richards, Sol. Energ. Mat. Sol. C., 2006, **90**, 1189-1207.

5 W. Shockley and H. J. Queisser, J. Appl. Phys., 1961, **32**, 510-519.

6 M. B. Spitzer and H.P. Jenssen. Sol. Energ. Mat. Sol. C., 2013, **108**, 241-245.

7 D. Q. Chen, Y.S. Wang and M. C. Hong, Nano Energy, 2012, **1**, 73-90.

8 L. Zhao, L. L. Han and Y.H. Wang, Opt. Mater. Express, 2014, **4**, 1456-1464.

9 T. Trupke, M. A. Green and P. Würfel, J. Appl. Phys., 2002, **92**, 1647-1668.

10 W. J. Zhu, D. Q. Chen, L. Lei, J. Xu, and Y. S. Wang, Nanoscale, 2014, **6**, 10500-10504.

11 Q. Y. Zhang, G. F. Yang and Z. H. Jiang, Appl. Phys. Lett., 2007, **91**, 051903.

12 V. D. Rodríguez, V. K. Tikhomirov, J. Méndez-Ramos, A. C. Yanes and V. V. Moshchalkov, Sol. Energ. Mat. Sol. C., 2014, **122**, 46-50.

13 K. Deng, T.Gong, L.Hu, X.Wei, Y.Chen and M.Yin, Opt. Express, 2011, **19**, 1749-1754.

14 H. Jing, C. F. Guo, G. G. Zhang, X.Y. Su, Z. Yang and J. H. Jeong, J. Mate. Chem., 2012, **22**, 13612-13618.

15 X. Y. Huang, D. C. Yu, and Q. Y. Zhang, J. Appl. Phys., 2009, **106**, 113521.

16 H. Zhang, X. Y. Liu, F. Y. Zhao, L. H. Zhang, Y. F. Zhang and H. Guo, Opt. Mater., 2012, **34**, 1034-1036.

17 S. Li, Z. Hou, Z. Cheng, H. Lian, P. Ma, C. Li and J. Lin, RSC Adv., 2013, **3**, 5491-5497.

18 N. M. Zhang, C. F. Guo, H. Jing and J. H. Jeong, Spectrochim. Acta A, 2013, **116**, 556-561.

19 W. J. Schipper and G. Blasse, J. Alloys. Compd., 1994, **203**, 267-269.

20 Q. Zhang, J. Wang, G. Zhang and Q. Su, J. Mater. Chem., 2009, **19**, 7088-7092.

21 Q. Y.Zhang and X. Y.Huang, Prog. Mater. Sci., 2010, **55**, 353-427.

22 D. Geng, G. Li, M. Shang, C. Peng, Y. Zhang, Z. Cheng and J. Lin, Dalton Trans., 2012, **41**, 3078-3086.

23 Y. Li, J. Wang, W. Zhou, G. Zhang, Y. Chen and Q. Su, Appl. Phys. Express, 2013, **6**, 082301.

24 X. Liu, Y. Teng, Y. Zhuang, J. Xie, Y. Qrao, G. Dong, D. Chen and J. Qiu, Opt. Lett., 2009, **34**, 3565-3567.

25 P. Vergeer, T. J. H. Vlugt, M. H. F. Kox, M. I. Den Hertog, J. P. J. M. Van der Eerden, and A. Meijerink, Phys. Rev. B, 2005, **71**, 014119.

26 R. Yu, S. Zhong, N.Xue, H. Li and H.Ma, Dalton Trans., 2014, **43**,10969-10976.

27 J. D. Chen, H. Guo, Z. Q. Li, H. Zhang and Y. X. Zhuang, Opt. Mater., 2010, **32**, 998-1001.

28 H. Lin, S. Zhou, H. Teng, Y. Li, W. Li, X. Hou, and T. Jia, J. Appl. Phys., 2010, **107**, 043107.

29 J. Ueda and S. Tanabe, J. Appl. Phys., 2009, **106**, 043101.

30 E. van der Kolk, O. M. Ten Kate, J. W. Wiegman, D. Biner and K. W. Krämer, Opt. Mater., 2011, **33**, 1024.

31 D. W. Cooke, R. E. Muenchausen, B. L. Bennett, K. J. McClellan and A.M. Portis, J. Lumin., 1998, **79**, 185-190.

32 Y. Zhu, Z. Sun, Z. Yin, H. Song, W. Xu, Y.Wang, L. Zhang and H. Zhang, Dalton Trans., 2013,**42**, 8049-8057.

33 C. F. Guo, H. Jing and T. Li, RSC adv., 2012, **2**, 2119-2122.

34 L. L. Han, Y. H. Wang, Y. Z. Wang, J. Zhang and Y. Tao, J. Alloy. Compd., 2013, **551**, 485-489.

35 I.A.A. Terra, L.J. Borrero-González, T. R. Figueredo, J. M. P. Almeida, A. C. Hernandes, L. A. O. Nunes and O. L. Malta, J. Lumin., 2012, **132**, 1678-1682.

Figure captions:

Fig. 1 XRD patterns of phosphors $Ba_2Y(BO_3)_2Cl$: Tb^{3+}, $Ba_2Y(BO_3)_2Cl$: Tb^{3+}, Yb^{3+} and $Ba_2Y(BO_3)_2Cl$: Ce^{3+}, Tb^{3+}, Yb^{3+} along as well with the standard profile for $Ba_2Yb(BO_3)_2Cl$ (JCPDS card No.79-0967).

Fig. 2. (**a**) PLE spectra (λ_{em} = 972 and 542 nm) and Vis-NIR PL spectrum (λ_{ex} = 486 nm) of sample $Ba_2Y(BO_3)_2Cl$: *0.03*Tb^{3+}, *0.20*Yb^{3+}; (**b**) PLE spectra (λ_{em} = 972 and 417 nm) and Vis-NIR PL spectrum (λ_{ex} = 355 nm) of sample $Ba_2Y(BO_3)_2Cl$: *0.03*Ce^{3+}, *0.20*Yb^{3+} and dependence of normalized integrated PL intensity in Vis and NIR region on Yb^{3+} concentration *x* in $Ba_2Y(BO_3)_2Cl$: *0.03*Tb^{3+}, *x*Yb^{3+} **(c)** and $Ba_2Y(BO_3)_2Cl$: *0.03*Ce^{3+}, *x*Yb^{3+} **(d)**.

Fig. 3 Decay lifetime of **(a)** Tb^{3+}: $^5D_4 \rightarrow {}^7F_5$ (542 nm) luminescence in $Ba_2Y(BO_3)_2Cl$: *0.03*Tb^{3+}, *x*Yb^{3+} under excitation of 486 nm and **(b)** Ce^{3+}: $5d \rightarrow 4f$ (417 nm) luminescence of $Ba_2Y(BO_3)_2Cl$: *0.03*Ce^{3+}, *x*Yb^{3+} under excitation of 375 nm; lifetime and energy transfer efficiency as function of Yb^{3+} concentrations in Tb^{3+}-*x*Yb^{3+} **(c)** and Ce^{3+}-*x*Yb^{3+} **(d)** co-doped $Ba_2Y(BO_3)_2Cl$.

Fig. 4 (**a**) PLE and (**b**) PL spectra of $Ba_2Y(BO_3)_2Cl$: *0.03*Ce^{3+}, *0.03*Tb^{3+}, *x*Yb^{3+} (*x*=0, 0.01, 0.05, 0.10, 0.20, 0.30) samples as functions of NIR emission center Yb^{3+} concentration *x*. Inset of **(b)** shows the dependence of Vis and NIR normalized integrated emission intensity on Yb^{3+} concentration *x*.

Fig. 5 Decay curves of (**a**) Ce^{3+}: $5d \rightarrow 4f$ (417 nm) emission in $Ba_2Y(BO_3)_2Cl$: *0.03*Ce^{3+}, *0.03*Tb^{3+}, *x*Yb^{3+} (*x*=0, 0.01, 0.05, 0.10, 0.20, 0.30) under excitation of 375 nm and (**b**) Tb^{3+}: $^5D_4 \rightarrow {}^7F_5$ (542 nm) emission under excitation of 355 nm; the variation trend of lifetime (Ce^{3+} and Tb^{3+}) and ET efficiency of ($Ce^{3+} \rightarrow Tb^{3+}/Yb^{3+}$ and $Tb^{3+} \rightarrow Yb^{3+}$) are shown in **(c)** and **(d)**.

Fig. 6 Schematic energy level diagram and the possible ET progresses in Ce^{3+}-Tb^{3+}-Yb^{3+} tri-doped $Ba_2Y(BO_3)_2Cl$ phosphor.

Fig. 7 The NIR emission spectra of (a) $Ba_2Y(BO_3)_2Cl$: *0.03*Tb^{3+}, *0.20*Yb^{3+}; (b) $Ba_2Y(BO_3)_2Cl$: *0.03*Ce^{3+}, *0.20*$Yb^{3+}$and (c) $Ba_2Y(BO_3)_2Cl$: *0.03*Ce^{3+}, *0.03*Tb^{3+}, *0.20*Yb^{3+} phosphors.

Figures:

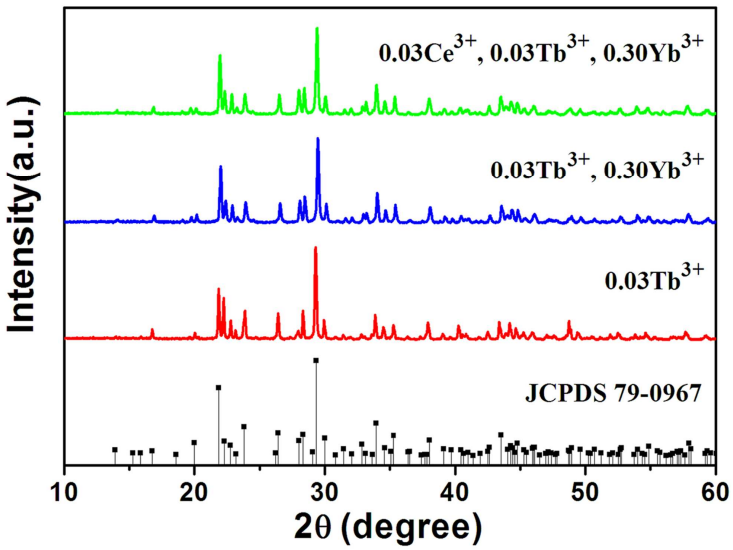

Fig. 1 XRD patterns of phosphors $Ba_2Y(BO_3)_2Cl$: Tb^{3+}, $Ba_2Y(BO_3)_2Cl$: Tb^{3+}, Yb^{3+} and $Ba_2Y(BO_3)_2Cl$: Ce^{3+}, Tb^{3+}, Yb^{3+} along as well with the standard profile for $Ba_2Yb(BO_3)_2Cl$ (JCPDS card No.79-0967).

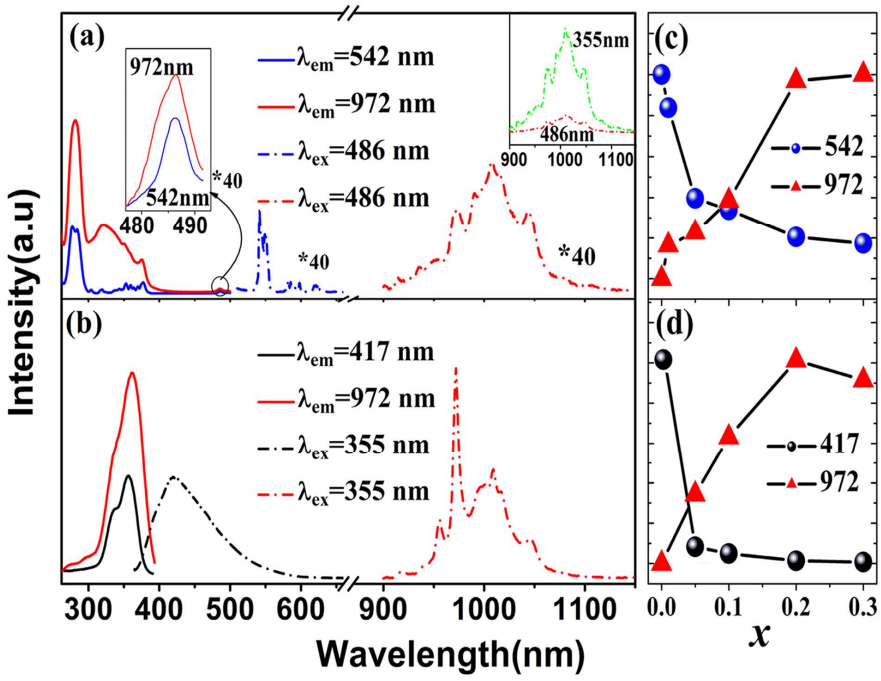

Fig. 2. (**a**) PLE spectra (λ_{em} = 972 and 542 nm) and Vis-NIR PL spectrum (λ_{ex} = 486 nm) of sample $Ba_2Y(BO_3)_2Cl$: *0.03*Tb^{3+}, *0.20*Yb^{3+}; (**b**) PLE spectra (λ_{em} = 972 and 417 nm) and Vis-NIR PL spectrum (λ_{ex} = 355 nm) of sample $Ba_2Y(BO_3)_2Cl$: *0.03*Ce^{3+}, *0.20*Yb^{3+} and dependence of normalized integrated PL intensity in Vis and NIR region on Yb^{3+} concentration *x* in $Ba_2Y(BO_3)_2Cl$: *0.03*Tb^{3+}, *x*Yb^{3+} **(c)** and $Ba_2Y(BO_3)_2Cl$: *0.03*Ce^{3+}, *x*Yb^{3+} **(d)**.

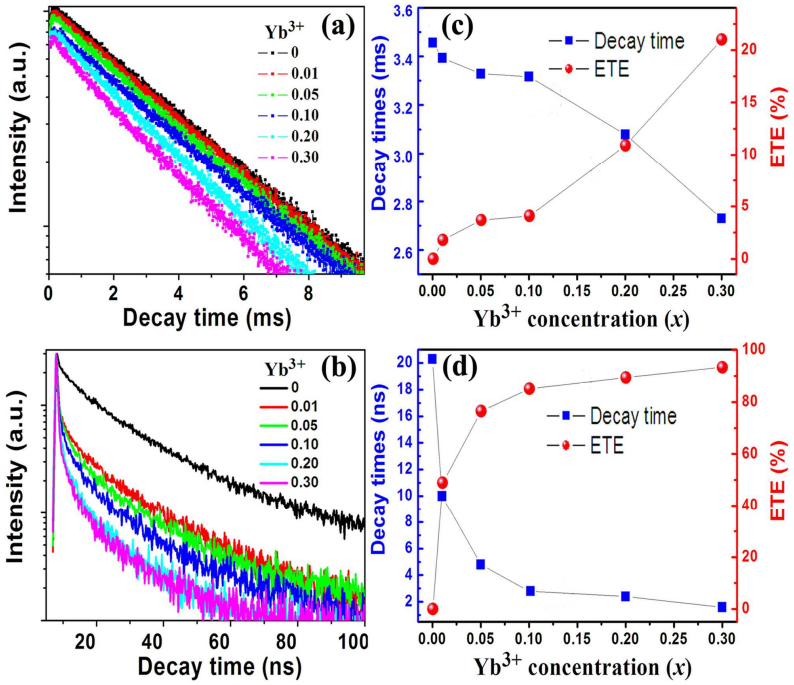

Fig. 3 Decay lifetime of **(a)** Tb^{3+}: $^5D_4 \rightarrow {}^7F_5$ (542 nm) luminescence in $Ba_2Y(BO_3)_2Cl$: *0.03*Tb^{3+}, *x*Yb^{3+} under excitation of 486 nm and **(b)** Ce^{3+}: $5d \rightarrow 4f$ (417 nm) luminescence of $Ba_2Y(BO_3)_2Cl$: *0.03*Ce^{3+}, *x*Yb^{3+} under excitation of 375 nm; lifetime and energy transfer efficiency as function of Yb^{3+} concentrations in Tb^{3+}-*x*Yb^{3+} **(c)** and Ce^{3+}-*x*Yb^{3+} **(d)** co-doped $Ba_2Y(BO_3)_2Cl$.

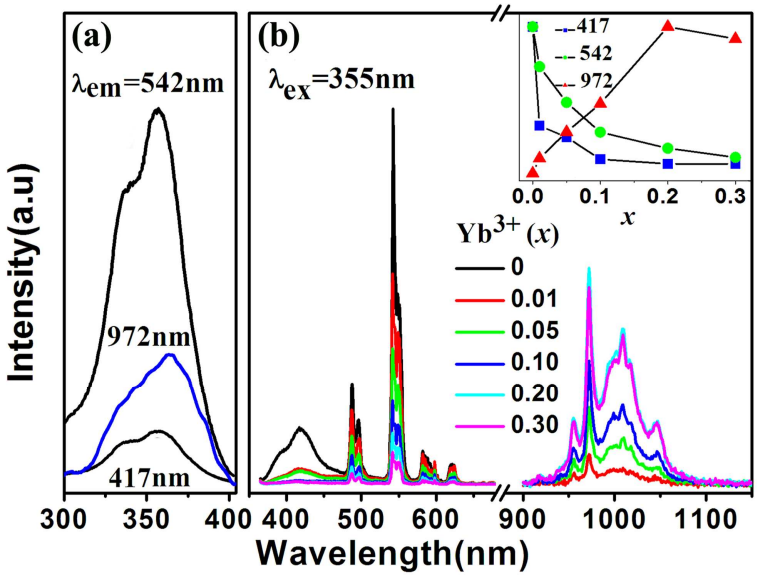

Fig. 4 (**a**) PLE and (**b**) PL spectra of $Ba_2Y(BO_3)_2Cl$: *0.03*Ce^{3+}, *0.03*Tb^{3+}, *x*Yb^{3+} (*x*=0, 0.01, 0.05, 0.10, 0.20, 0.30) samples as functions of NIR emission center Yb^{3+} concentration *x*. Inset of **(b)** shows the dependence of Vis and NIR normalized integrated emission intensity on Yb^{3+} concentration *x*.

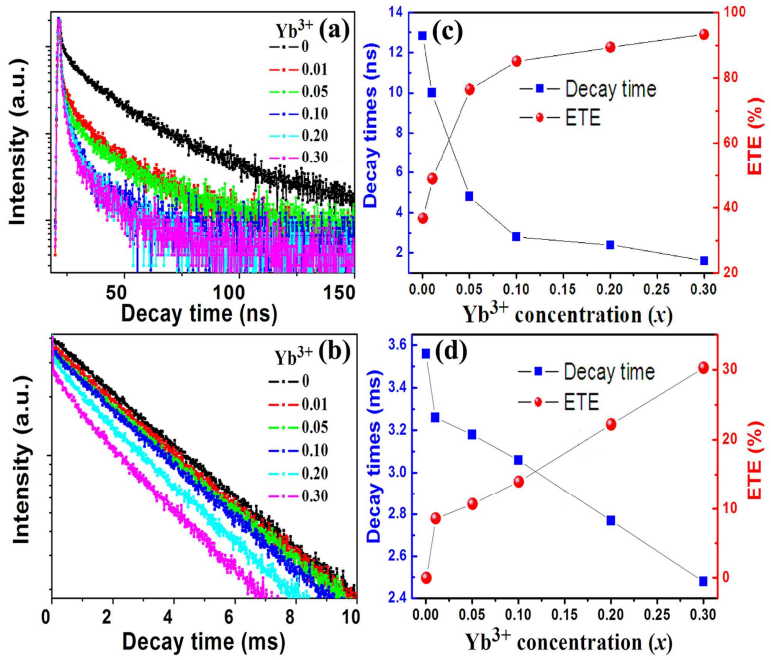

Fig. 5 Decay curves of (**a**) Ce^{3+}: *5d*→*4f* (417 nm) emission in $Ba_2Y(BO_3)_2Cl$: *0.03*Ce^{3+}, *0.03*Tb^{3+}, *x*Yb^{3+} (*x*=0, 0.01, 0.05, 0.10, 0.20, 0.30) under excitation of 375 nm and (**b**) Tb^{3+}: $^5D_4$→$^7F_5$ (542 nm) emission under excitation of 355 nm; the variation trend of lifetime (Ce^{3+} and Tb^{3+}) and ET efficiency of (Ce^{3+}→Tb^{3+}/Yb^{3+} and Tb^{3+}→Yb^{3+}) are shown in **(c)** and **(d)**.

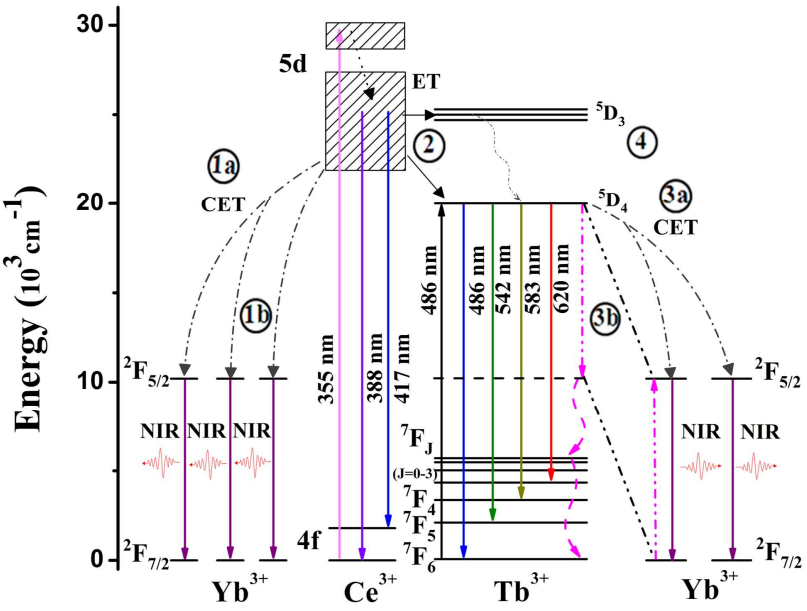

Fig. 6 Schematic energy level diagram and the possible ET progresses in Ce^{3+}-Tb^{3+}-Yb^{3+} tri-doped $Ba_2Y(BO_3)_2Cl$ phosphor.

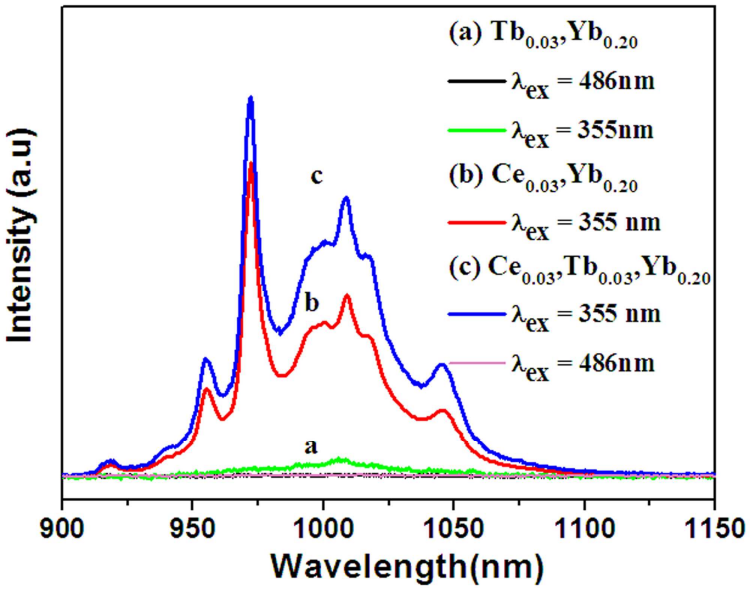

Fig. 7 The NIR emission spectra of (a) $Ba_2Y(BO_3)_2Cl$: *0.03*Tb^{3+}, *0.20*Yb^{3+}; (b) $Ba_2Y(BO_3)_2Cl$: *0.03*Ce^{3+}, *0.20*Yb^{3+} and (c) $Ba_2Y(BO_3)_2Cl$: *0.03*Ce^{3+}, *0.03*Tb^{3+}, *0.20*Yb^{3+} phosphors.

Enhanced near-infrared emission by co-doping Ce^{3+} in $Ba_2Y(BO_3)_2Cl$: Tb^{3+}, Yb^{3+} phosphor

Jin Zhao, Chongfeng Guo* and Ting Li

National Key Laboratory of Photoelectric Technology and Functional Materials (Culture Base) in Shaanxi Province, National Photoelectric Technology and Functional Materials & Application of Science and Technology International Cooperation Base, Institute of Photonics & Photon-Technology, Northwest University, Xi'an 710069, China

---

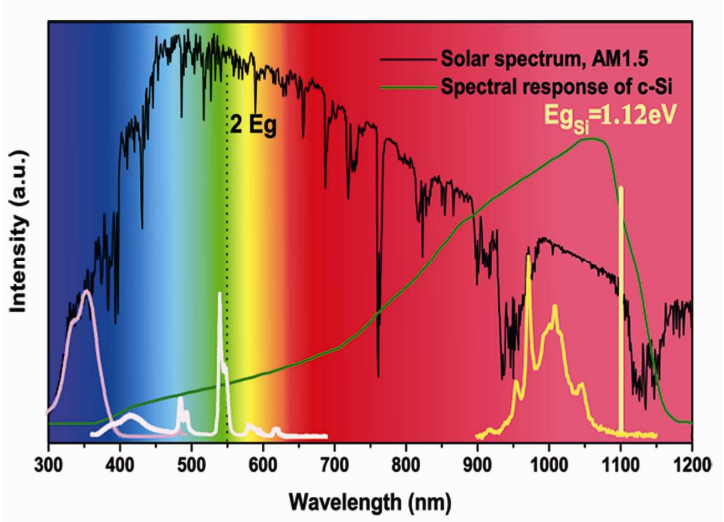

$Ba_2Y(BO_3)_2Cl$: Ce^{3+}, Tb^{3+}, Yb^{3+} with intense near-infrared emission and broad-band absorption in n-UV region is a promising down-conversion solar spectral convertor to enhance the efficiency of the silicon solar cells.